

Geophysical Research Letters[®]



RESEARCH LETTER

10.1029/2023GL106637

Radio Occultation Measurements of Europa's Ionosphere From Juno's Close Flyby

Key Points:

- Europa's ionosphere was detected from Juno's X-band Doppler data via NASA's Deep Space Network during a close encounter in 2022
- Peak densities were $4,000 \pm 3,700 \text{ cm}^{-3}$ (3σ) at 22 km altitude during ingress and $6,000 \pm 3,000 \text{ cm}^{-3}$ (3σ) at 320 km during egress
- The Juno ionospheric profiles are consistent with Galileo measurements, and show a dependence on solar zenith and magnetospheric ram angles

Supporting Information:

Supporting Information may be found in the online version of this article.

Correspondence to:

M. Parisi,
marzia.parsi@jpl.nasa.gov

Citation:

Parisi, M., Caruso, A., Buccino, D. R., Gramigna, E., Withers, P., Gomez-Casajus, L., et al. (2023). Radio occultation measurements of Europa's ionosphere from Juno's close flyby. *Geophysical Research Letters*, 50, e2023GL106637. <https://doi.org/10.1029/2023GL106637>

Received 2 OCT 2023

Accepted 9 NOV 2023

Author Contributions:

Conceptualization: M. Parisi, D. R. Buccino, P. Steffes, P. Tortora, S. Levin, S. Bolton













Data curation: D. R. Buccino

Formal analysis: M. Parisi, A. Caruso, E. Gramigna, P. Withers, L. Gomez-Casajus, D. A. Coffin, M. Zannoni

Funding acquisition: S. Levin, S. Bolton

© 2023 Jet Propulsion Laboratory, California Institute of Technology and The Authors. Government sponsorship acknowledged.

This is an open access article under the terms of the [Creative Commons Attribution-NonCommercial License](https://creativecommons.org/licenses/by-nc/4.0/), which permits use, distribution and reproduction in any medium, provided the original work is properly cited and is not used for commercial purposes.

M. Parisi¹ , A. Caruso² , D. R. Buccino¹ , E. Gramigna² , P. Withers³ , L. Gomez-Casajus⁴ , D. A. Coffin³, R. S. Park¹ , P. Steffes⁵ , P. Tortora^{2,4} , M. Zannoni^{2,4} , S. Levin¹ , and S. Bolton⁶ 

¹Jet Propulsion Laboratory, California Institute of Technology, Pasadena, CA, USA, ²Dipartimento di Ingegneria Industriale, Alma Mater Studiorum—Università di Bologna, Forli, Italy, ³Boston University, Boston, MA, USA, ⁴Centro Interdipartimentale di Ricerca Industriale Aerospaziale, Alma Mater Studiorum - Università di Bologna, Forli, Italy, ⁵School of Electrical and Computer Engineering, Georgia Institute of Technology, Atlanta, GA, USA, ⁶Southwest Research Institute, San Antonio, TX, USA

Abstract On 29 September 2022 the Juno spacecraft flew within 354 km of Europa's surface while several instruments probed the moon's surroundings. During the close flyby, radio occultations were performed by collecting single-frequency Doppler measurements. These investigations are essential to the study of Europa's ionosphere and represent the first repeat sampling of any set of conditions since the Galileo era. Ingress measurements resulted in a marginal detection with a peak ionospheric density of $4,000 \pm 3,700 \text{ cm}^{-3}$ (3σ) at 22 km altitude. A more significant detection emerged on egress, with a peak density of $6,000 \pm 3,000 \text{ cm}^{-3}$ (3σ) at 320 km altitude. Comparison with Galileo measurements reveals a consistent picture of Europa's ionosphere, and confirms its dependence on illumination conditions and position within Jupiter's magnetosphere. However, the overall lower densities measured by Juno suggest a dependence on time of observation, with implications for the structure of the neutral atmosphere.

Plain Language Summary On 29 September 2022, NASA's Juno spacecraft flew very close to Jupiter's moon Europa. During the encounter, a radio occultation experiment was performed, where radio signals are exchanged between the spacecraft and ground stations as the former sets behind or rises from the moon as seen from the Earth. The scope of this experiment was studying the ionosphere of Europa, a layer of electrons and ions surrounding the moon. The Juno measurements confirmed the presence of the layer, with a structure similar to the one observed by the Galileo mission in the late 1990s.

1. Introduction

In the pre-Galileo era, the only instance of atmospheric detection at a Galilean moon were the observations made by Pioneer 10 around Io (Kliore et al., 1974). Two decades later, compelling Hubble Space Telescope observations emerged, suggesting that Europa may also possess an atmosphere composed of atomic oxygen, among other species, likely originating from frozen surface water ice and created by particle impacts and radiolysis (Hall et al., 1995). In the late 1990s and early 2000s, the Galileo spacecraft performed observations of Jupiter and all four of its largest moons (Kliore, 1998). An experiment was planned to search for an atmosphere on Europa as the spacecraft was occulted on three occasions. The analysis revealed the presence of ionization during five of the six measurements. The maximum electron densities ranged from 6,000 to 11,000 cm^{-3} near the surface (Kliore et al., 1997). An average profile was computed, with a peak density of about 9,000 cm^{-3} and plasma scale heights of 240 and 440 km below and above 300 km, respectively. Various scenarios for the composition and properties of Europa's atmosphere were discussed by Kliore et al. (1997). The presence of molecular species such as O_2 , H_2O , H , H_2 , OH , and O was considered, and the required neutral density for sustaining the observed electron density was estimated around 10^8 cm^{-3} at the surface. The analysis also addressed the issue of optical depth and column density, suggesting values below the limits set by previous studies. Overall, Galileo data indicated the presence of a thin ionosphere and atmosphere around Europa, likely consisting of a mixture of molecular and atomic species.

During its extended phase, the Juno mission is poised to undertake a range of scientific endeavors. The spacecraft has already embarked on close flybys of Ganymede (Hansen et al., 2022) and Europa, with one visit to each moon. Furthermore, Juno is anticipated to approach Io at close proximity in late 2023 and early 2024. The Juno rendezvous to Europa occurred on 29 September 2022, during which the spacecraft disappeared behind the moon

Investigation: M. Parisi, P. Withers, D. A. Coffin, P. Steffes, S. Levin, S. Bolton
Methodology: M. Parisi, A. Caruso, E. Gramigna, P. Withers, L. Gomez-Casajus, D. A. Coffin, M. Zannoni
Project Administration: R. S. Park, P. Steffes, P. Tortora, S. Levin, S. Bolton
Resources: D. R. Buccino, R. S. Park
Software: M. Parisi, A. Caruso, E. Gramigna, P. Withers, L. Gomez-Casajus, P. Tortora, M. Zannoni
Supervision: R. S. Park, P. Steffes, P. Tortora, S. Levin, S. Bolton
Validation: M. Parisi, A. Caruso, E. Gramigna, L. Gomez-Casajus, M. Zannoni
Writing – original draft: M. Parisi
Writing – review & editing: M. Parisi, A. Caruso, D. R. Buccino, E. Gramigna, P. Withers, R. S. Park, P. Steffes, P. Tortora

as viewed from ground-based antennas. The spacecraft collected occultation measurements using a coherent X-band link with NASA's Deep Space Network (DSN) using its Medium Gain Antenna (MGA). Observations were conducted at new solar zenith (SZA) and magnetospheric ram angles, as well as geographic locations, compared to Galileo.

Understanding the characteristics of Europa's ionosphere holds further significance in view of the upcoming Europa Clipper mission. The spacecraft will make observations of the moon's ionosphere on several occasions in a similar configuration to that of Juno's occultations (Mazarico et al., 2023). It has been suggested that the ionosphere affects radar observations of the moon's surface and subsurface (Grima et al., 2015). Comprehending the behavior of the ionosphere will enable the calibration of its effects on remote-sensing measurements and mitigate distortions or disruptions in the observations. Here we present the analysis of Juno's radio occultation experiment at Europa and provide a discussion of the results obtained, considering our current understanding of the moon's thin ionosphere.

2. The Europa Occultation of the Juno Spacecraft

During the Europa occultation experiment (labeled as E45, as it occurred on orbit 45), the Juno Gravity Science Instrument (Asmar et al., 2017) employed a single-frequency X-band (7.2–8.4 GHz) radio link between the spacecraft and DSN's 70-m antenna in Goldstone, California (DSS-14). The experiment used a two-way configuration, where a ground station transmits a signal to the spacecraft, which receives it and phase-coherently relays it back. Figure 1 shows the occultation from different viewpoints. Ionospheric measurements of Europa were obtained while Juno was positioned behind Europa as observed from the ground, and radio signals passed through the moon's ionosphere. The ingress (E45N) and egress (E45X) points were located at 39°S, 167°E and 2.6°N, 349°E European latitude and longitude, respectively. The ray impact velocity was 15.5 km s⁻¹. Both occultations occurred near the day/night transition (terminator) and on the edges of the magnetospheric wake, in which the satellite interacts with the flow of charged particles from Jupiter's magnetosphere. The egress occultation is categorized as an “in situ” experiment, indicating that the spacecraft was situated within Europa's ionosphere during the observations (Figure 1). This has notable implications for data analysis, which will be elaborated in later sections.

In order to accommodate concurrent observations by other instruments, the spacecraft was turned from its gravity science attitude, preventing the use of Juno's High Gain Antenna (HGA) and dual-frequency for collecting Doppler data. The MGA was employed instead, resulting in a lower signal to noise ratio (SNR), and periodical effects on the Doppler data due to the antenna offset with respect to the Juno spin axis. To ensure signal acquisition during the occultation egress, a snap-lock technique was employed as in the case of Ganymede (Buccino et al., 2022). Instead of executing an uplink acquisition sweep, the technique relied on precisely targeting the spacecraft transponder's best lock frequency. The snap-lock procedure took into account predictions of the oscillator frequency based on its temperature and estimated Doppler shift in the uplink signal, successfully re-locking the transponder within 4 s after egress, corresponding to an altitude of approximately 52 km. Due to the high spacecraft velocity (approximately 23.6 km/s), the technique prevented the loss of occultation and gravity data during egress.

3. Analysis Methods and Data Set

Radio occultation methods involve the retrieval of bending angles exhibited by radio signals while they traverse planetary atmospheres and ionospheres. As the refractive index within these media deviates from unity, the radio signal experiences refraction, ceasing to propagate along straight trajectories and instead bending in accordance with the characteristics of the medium. This effect introduces phase delays and hence frequency shifts as compared to a signal propagating in vacuum. By accurately measuring the frequency shifts from ground stations one can extract information about the optical medium. Radio occultations have been used for decades to investigate the atmosphere of distant bodies as well as the Earth's. Early examples are found in Kliore et al. (1965), Phinney and Anderson (1968), and Fjeldbo and Eshelman (1968). Typically, the outcome is the retrieval of electron density profiles for ionospheres, as well as number density, pressure, and temperature for the neutral atmosphere. These properties are obtained as a function of altitude above the surface of the body. During a spacecraft's flyby, the recorded Doppler shift on the received signal carries information about different effects.

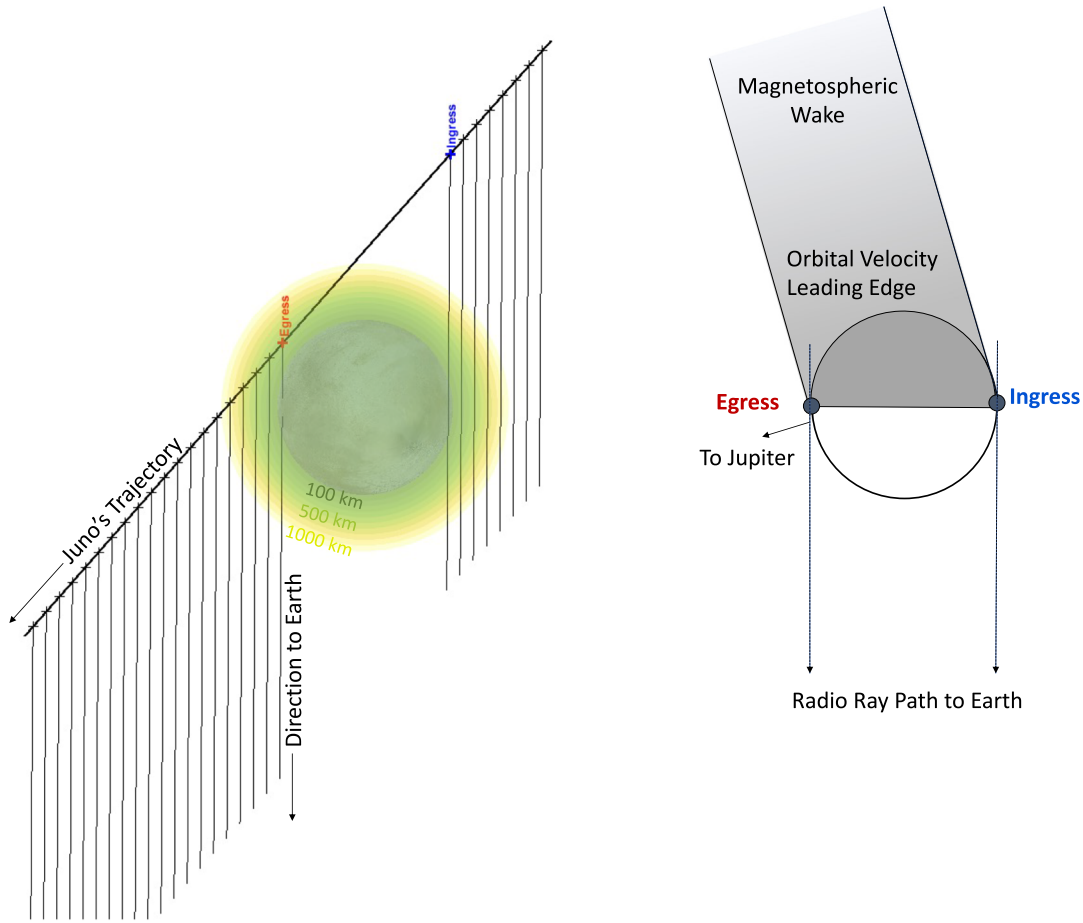


Figure 1. Schematics of Juno's occultations by Europa. The plot on the left shows the evolution of Juno's trajectory (ticks are generated every 15 s) and highlights the in-situ geometry of the egress occultation. The plot on the right shows the relative position of Europa with respect to Jupiter's magnetosphere. Both occultations occurred near the terminator.

These include the spacecraft's motion, the neutral atmosphere, and the presence of charged particles (Equation 1) (Dalba & Withers, 2019):

$$f_R = f_T - \frac{f_T}{c} \frac{d}{dt} \int dl - \frac{f_T \kappa}{c} \frac{d}{dt} \int n dl + \frac{e^2}{8\pi^2 m_e \epsilon_0 c f_T} \int N_e dl, \quad (1)$$

where f_R is the received frequency, f_T is the transmitted frequency, c is the speed of light, dl is the infinitesimal element of the ray path, κ is the refractive volume of the neutral atmosphere, n is the number density of neutral molecules, e is the elementary charge, m_e is the electron mass, ϵ_0 is the permittivity in vacuum and N_e is the electron density. If the effect of the trajectory can be adequately accounted for by precisely determining the spacecraft's motion (Equation 1 of Schinder et al., 2015; Equation 8 of Withers & Moore, 2020), it becomes possible to isolate the impact of neutrals and charged particles. When a radio signal is traversing a region rich in electrons and ions, the refractive index is less than unity and the phase is advancing with respect to one traveling entirely in vacuum. The phase changes are proportional to the electron density and inversely proportional to the square of the frequency. The behavior of radio signals in ionospheres is dispersive, as the corresponding Doppler shift depends on frequency. It follows that dual-frequency observations are typically preferred for investigating planetary ionospheres, as illustrated by Buccino et al. (2022). We follow instead approaches for two-way, single-frequency occultations.

The two-way Juno Doppler data received at DSS-14 during the Europa occultation was recorded using the DSN Open-Loop Receivers, which directly recorded the antenna voltages in terms of I/Q samples using a fixed sample rate. As outlined in Buccino et al. (2022), the data processing can be performed a posteriori from the time of

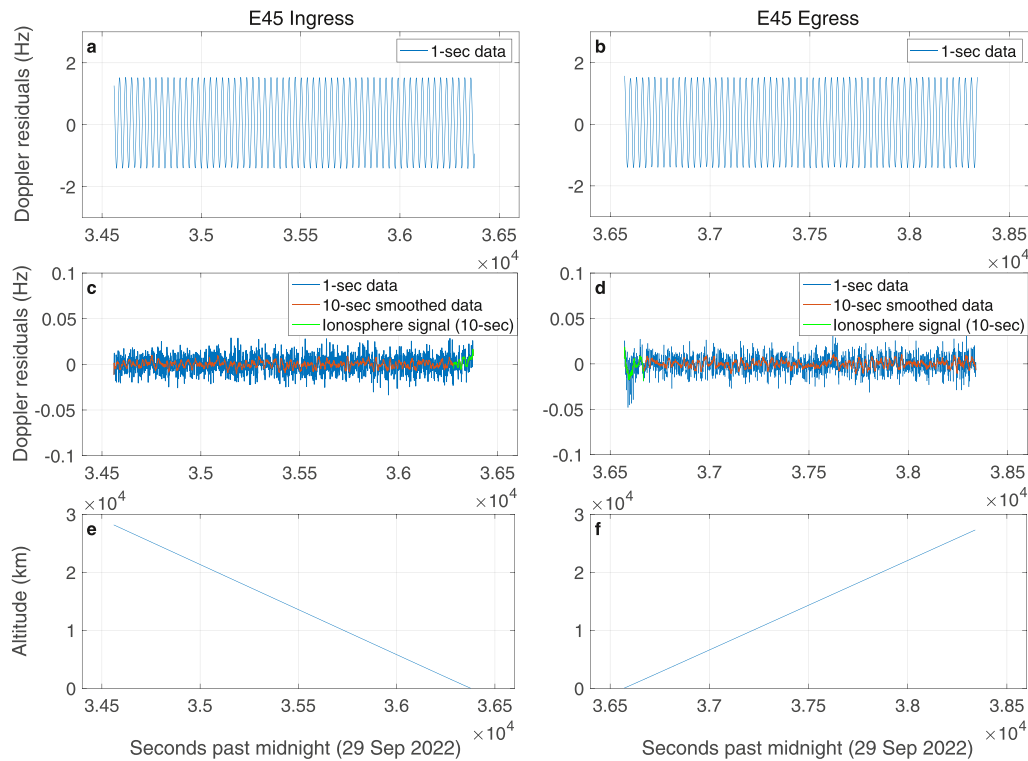


Figure 2. Doppler residuals during the ingress (a), (c) and egress (b), (d) Europa occultation. The residuals before calibration of the Medium Gain Antenna offset (a), (b) show significant periodic signatures. The residuals after calibration (c), (d) show a zero-mean, white noise behavior throughout the baseline and a clear ionospheric signature close to the occultation points. The altitude of the ray path over Europa's surface is shown in panels e, f.

acquisition. This configuration has at least two advantages: (a) it allows the user to always refer back to the raw data and change the data processing parameters for optimization purposes; (b) in the specific case of radio occultations, it helps maintaining lock with the received signal, task that is especially challenging when the spacecraft is coming out of the occultation. From a sample rate of 1 kHz, frequency observables were obtained from open-loop data samples using a spectrally optimized fast Fourier transform technique (Paik & Asmar, 2010; Togni et al., 2021) at an integration time of 1 s. The corresponding vertical resolution was 15.5 km.

The integration time was chosen not to alias the Doppler spin signature caused by the MGA, obtain an adequate vertical resolution, and minimize the thermal noise on the observables. The use of the MGA entailed higher thermal noise on the data as compared to observations carried out with the HGA (Buccino et al., 2022). For reference, the average SNR was around 34 dB-Hz during the occultation (Figure S1 in Supporting Information S1).

The occultations required careful calibration of the periodic signatures on the Doppler data. Figure 2 shows the E45 data -set after the effect of the spacecraft's motion was removed (Doppler residuals). Before calibrating for the spinning effect (panels a, b), periodical fluctuations up to 1.5 Hz amplitude were present. Since the periodicity of this interference is related to the Juno spin rate (2 RPM), it was removed by applying sinusoidal corrections (panels c, d of Figure 2, Text S1 in Supporting Information S1). The red lines represent data smoothing of the Doppler residuals at 10 s, and the green lines emphasize the ionospheric signal near ingress and egress. Furthermore, an additional calibration step on the Doppler data was performed. A linear bias was removed from the residuals, as is often done to compensate for interplanetary plasma effects (Gramigna et al., 2023; Kliore et al., 1997). The bias was calculated separately for ingress and egress, using data points corresponding to ray path altitudes above 1,500 km (called the baseline, Figures 2e and 2f), where it is assumed that the spacecraft's signals were propagating well outside Europa's ionosphere (Text S1 in Supporting Information S1). The detected linear trends were of order 10^{-7} – 10^{-6} Hz s^{-1} , indicating that other dispersive effects were quiet during the occultation (e.g., the spacecraft was near solar opposition). We also observed that the ionospheric profiles were not significantly

affected by the choice of the baseline ($\ll 1\sigma$), as long as the cutoff was at least 1,500 km. As described in Buccino et al. (2022), other sources of noise (e.g., instrumentation, Earth's ionosphere) were calibrated when possible but overall did not have a significant impact on the results. Lastly, models (Moirano et al., 2021; Phipps et al., 2021) predict the radio link did not propagate through the Io Plasma Torus during the E45 flyby.

3.1. Ingress Occultation and Abel Transform

During the ingress occultation, the spacecraft was located outside of the ionosphere. Since the occultation was conducted in two-way mode, the signal traversed the ionosphere twice. An exhaustive description of the methodology used to analyze the ingress data can be found in Withers and Moore (2020), referred to as WM20 henceforth. It is assumed that the uplink and downlink signals traversed the same portion of the ionosphere, which implies that the spacecraft was much closer to the target object (Europa) than it was to Earth. Another assumption is that of local spherical symmetry. As stated in Buccino et al. (2022), the latter can be justified by the small values of refractivity detected in the ionosphere (peaks of 10^{-9} – 10^{-8}). The rays experience negligible bending and can reasonably be considered to travel along straight trajectories, rendering the use of the Abel transform suitable. Under the assumption of local spherical symmetry, the ionosphere is still allowed to globally have a non-spherical shape, as indicated by models (Bagenal & Dols, 2020; Harris et al., 2022), and the assumption is held only for the limited portion of the ionosphere traversed by the radio signal (Text S3 and Figure S3 in Supporting Information S1). These conditions are met by Juno's occultation of Europa, and four equations with four unknowns (the two bending angles on uplink and downlink) can be written. These are the frequency residual, uplink impact parameter, downlink impact parameter, and bending angle relationships, corresponding to Equations. 38, 44, 50, and 56 of WM20.

Once the bending angles and impact parameters were calculated, we retrieved the refractive index μ of the ionosphere. If R , a , and α are the ray path radial distance, impact parameter and bending angle, respectively, as shown in Figure 1 of WM20, then for each observation j they are related by the Abel transform:

$$\pi \ln \mu(R_j) = - \int_{a=a_j}^{a=\infty} \ln \left\{ \frac{a}{a_j} + \left[\left(\frac{a}{a_j} \right)^2 - 1 \right]^{1/2} \right\} \frac{d\alpha}{da} da. \quad (2)$$

It is not possible to straightforwardly separate the effect of the ionosphere and neutral atmosphere with single-frequency occultations. However, in the case of Europa, the neutral atmosphere is very faint and its contribution to the signals' bending angles is negligible compared to the effect of the ionosphere. Thus, the electron density profile was directly obtained from the refractivity ν :

$$\nu_e = - \frac{e^2 N_e}{8\pi^2 m_e \epsilon_0 f_T^2} \quad (3)$$

where $\nu = \mu - 1$.

3.2. Egress Occultation and Analytical Ray Tracing

The assumptions that justify the use of an Abel transform would not hold for the in-situ geometry of the egress occultation. For this reason, we resorted to the use of analytical ray-tracing, which is briefly outlined in the following paragraphs. A complete and thorough description of the methodology can be found in Bourgoïn et al. (2019) and Caruso et al. (2023).

The core concept of this approach is to consider the atmosphere as composed of concentric shells, with the properties of the gas in each layer computed through an iterative procedure. Geometric optics approximation forms the foundation of this method, assuming that each sky frequency is associated with a ray path traversing the atmosphere. The ray path can be obtained analytically as explained in Bourgoïn et al. (2019) within the assumption of local spherical symmetry, where the refractive index inside a layer is a linear function of the planet's gravitational potential.

The problem consists of solving a set of nonlinear equations: for each value of sky frequency (Figure 2), we solve for the ray's initial direction and refractivity gradient inside the shells to ensure that the ray direction points

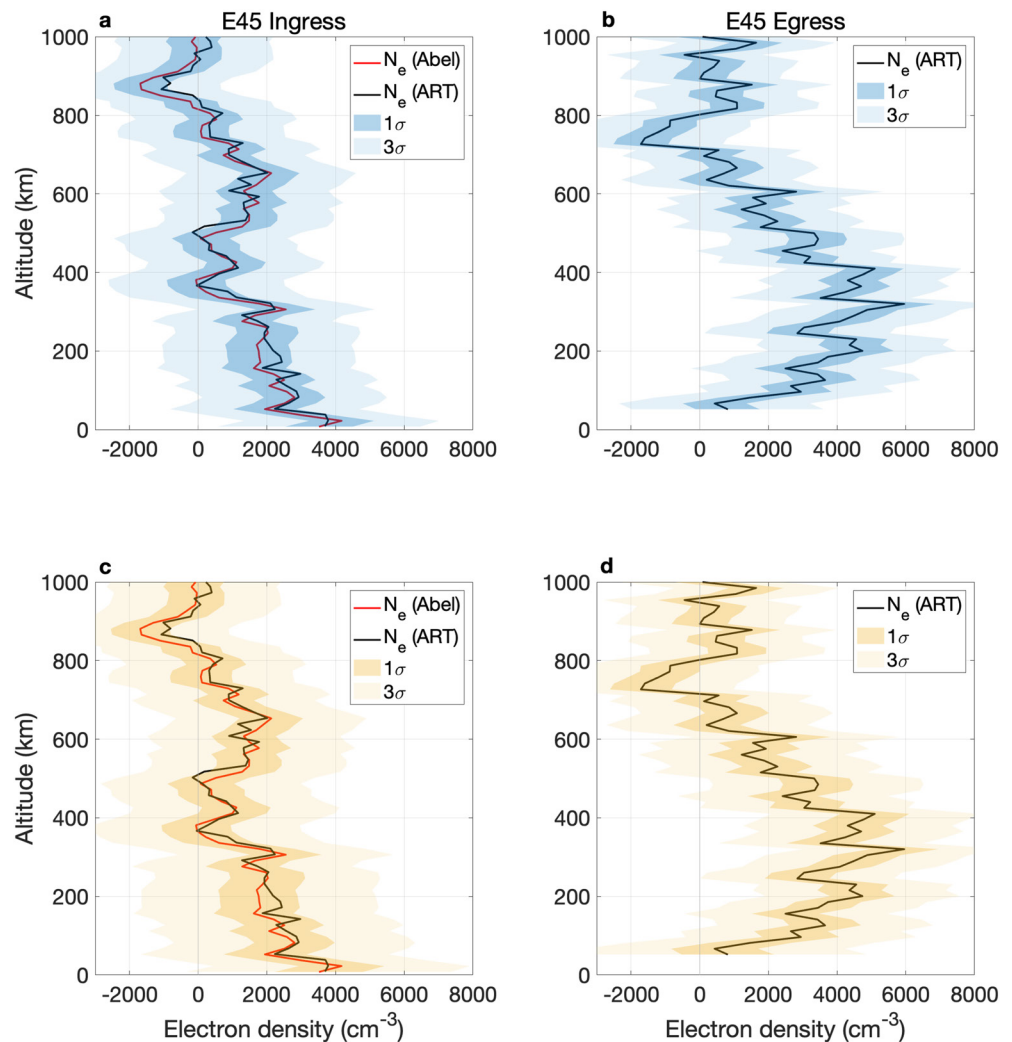


Figure 3. Vertical profiles of Europa's ionosphere. ART stands for analytical ray tracing, while Abel stands for the transform of the same name. Panels (a), (b) show the ingress and egress profiles, respectively. Formal uncertainty were calculated considering thermal noise only. Panels (c), (d) show the same profiles, but formal uncertainties were calculated considering also the effect of the gravity field of Europa.

toward the receiving antenna upon leaving the atmosphere and that the signal reaches the ground antenna with the recorded sky frequency. Once the refractivity gradient is computed within all the shells, we can obtain the complete refractivity profile and, consequently, the electron density using Equation 3.

4. Results

The Juno E45 data -set comprises a total of 1817 data points (at 1-s integration time) for the ingress portion of the occultation, with cut-off at 10:06:16.5 (UTC Earth Receive Time). The corresponding altitudes sampled by the radio signals range between approximately 30,000 and 7.5 km. Although loss of signal occurred after the cut-off time, the epoch was selected to avoid the effect of diffraction caused by the proximity to Europa's surface. A total of 1770 data points are available for egress, with reliable signal reacquisition occurring at 10:09:31.5 (UTC Earth Receive Time) and a lower bound on the altitude of the vertical profile of 52 km, well above the altitude threshold where diffraction is significant.

The Doppler residuals shown in Figures 2c and 2d were converted into vertical profiles of electron densities (cm^{-3}) using the Abel transform for ingress data and analytical ray tracing for locally symmetric atmospheres for both ingress and egress data, for validation purposes. The results of the data inversion are shown in Figure 3,

in terms of electron density N_e as a function of European altitude. The ionospheric profile retrieved during the ingress occultation (a, c) shows values below $3,000 \text{ cm}^{-3}$ throughout, until reaching a peak around $4,000 \text{ cm}^{-3}$ at an altitude of 22 km above the surface of Europa. As expected, the differences between the ingress profiles obtained using the Abel transform or analytical ray tracing are negligible ($<1\sigma$). On the egress occultation (b, d), the electron density profile obtained with ray tracing shows a bulge between altitudes of 200–400 km, reaching a maximum of $6,000 \text{ cm}^{-3}$ around altitude 320 km, while decreasing significantly at low altitudes ($<100 \text{ km}$). Egress results obtained with an Abel transform are not reported, as its application to the egress data set would be incorrect. Results in terms of Total Electron Content are available in Supporting Information S1.

It is crucial to accurately quantify the uncertainties in the measurement of the electron density profiles. The first source of noise discussed is associated with the lower SNR, resulting in higher thermal noise on Doppler observables. A straightforward technique for promptly estimating this effect is calculating the standard deviation of the electron density profile throughout the baseline ($h > 1,500 \text{ km}$), where the imprint of Europa's ionosphere is negligible. The approach yields a constant value of the standard deviation with altitude, as presented by Dalba and Withers (2019) for determining the accuracy on Titan's ionospheric profiles. A different approach involves the usage of Monte Carlo analyses, used to calculate the formal 1σ uncertainties (darker blue shaded areas in Figures 3a and 3b) as a function of altitude (Bourgoin et al., 2022; Gramigna et al., 2023). Gaussian random noise time-series, with standard deviation matching the observed noise levels outside Europa's ionosphere, were added to the original differential frequency residuals. This process allowed for the computation of multiple electron density profiles, used to estimate the error bars. When thermal fluctuations are the only source of noise, the estimated 3σ uncertainty (lighter blue shaded area in Figures 3a and 3b) displays values increasing toward lower altitudes, reaching a maximum of $3,000 \text{ cm}^{-3}$ for ingress and $2,800 \text{ cm}^{-3}$ for egress. When the uncertainties are compared to the peaks at $4,000 \text{ cm}^{-3}$ for ingress and $6,000 \text{ cm}^{-3}$ for egress, this would imply a clear detection of Europa's ionosphere on both occultation legs.

Radio occultations are usually performed during times where the spacecraft is not subject to uncalibrated effects in the Doppler shift, in order to avoid coupling the effect of charged particles and that of the gravity field on the spacecraft trajectory. Alternatively, the experiment could employ dual-frequency measurements to decouple the two effects. Neither scenario occurred during Juno Europa's occultation. The spacecraft was as close as 3,204 km to the surface of Europa during ingress, closest approach occurred about 95 s later at an altitude of 353.8 km, and egress occurred after only 8.5 s, with an altitude only 10 km higher. Thus, the effect of uncertainties in the knowledge of Europa's gravity field and Juno trajectory cannot be neglected, especially for the egress occultation. In order to account for this effect, a different Monte Carlo analysis was performed with different considerations. In addition to thermal noise, several trajectories for the Juno spacecraft were generated using 500 different quadrupole gravity fields, all compatible with the latest gravity field determination (Gomez Casajus et al., 2021) within 3σ . During these tests, the spacecraft state was always within 200 m in the normal direction and 100 m (1σ) in the transverse direction of the reconstructed trajectory by the Juno Navigation Team (2022). As a result, the formal uncertainties are higher, especially at lower altitudes and close to the surface during the egress occultation. The largest 3σ uncertainties are of order $3,850 \text{ cm}^{-3}$ on ingress and $4,300 \text{ cm}^{-3}$ on egress. On ingress the peak occurs in the region of maximum uncertainty at $4,000 \pm 3,700 (3\sigma) \text{ cm}^{-3}$. We characterized these results as a marginal detection of the ionosphere. On egress, the peaks occur at higher altitudes, and the corresponding uncertainties are $2,850\text{--}3,050 \text{ cm}^{-3} (3\sigma)$. This can be characterized as a stronger detection of the ionosphere.

5. Interpretation and Discussion

In this section we explore the possible dependence of ionospheric profiles on different parameters such as solar zenith angles, magnetospheric ram angle, solar cycle and European geographic location. Furthermore, we compare our observations to the six Galileo measurements of Europa's ionosphere (E4N/X, E6aN/X, and E6bN/X, where N stands for ingress and X for egress) as reported by Kliore et al. (1997) and McGrath et al. (2009) (Figure S4 in Supporting Information S1). The first aspect investigated is the location of the occultation points with respect to forcing sources. The Juno observations were characterized by SZA angles of 89.3° , 90.6° and ram angles of 101° , 80° for ingress and egress, respectively. Generally speaking, we classify $\text{SZA} = 0\text{--}90^\circ$ as “Day” and $90\text{--}180^\circ$ as “Night.” Similarly, ram angles $0\text{--}45^\circ$ are classified as “Nose,” $45\text{--}135^\circ$ as “Flanks” and $135\text{--}180^\circ$ as “Wake.” The Galileo profiles corresponded to SZA values between 85° and 95° , therefore the Juno values are intermediate. They might better be classified as terminator rather than splitting day and night precisely at 90° .

The only profile (out of 8) with absolutely zero densities is Galileo's E6aX in Night/Wake, which is where the smallest densities would be expected. On the other hand, the only Day/Wake profile (E6bN) has non-zero densities. A possible interpretation of these results is that appreciable ionospheric densities exist for all conditions except Night/Wake, which has implications for where neutral atmospheric densities must be non-zero and for plasma production and loss mechanisms. E4X and E45N are both Day/Flanks profiles. E4X has large densities ($10,000 \text{ cm}^{-3}$) that are confined to low altitudes ($<150 \text{ km}$). E45N has smaller densities ($4,000 \text{ cm}^{-3}$) that also look confined to low altitudes, however uncertainties might prevent us from making a definitive statement. It follows that the ionosphere observations appear somewhat repeatable in the Day/Flanks sector. E4N and E45X are both Night/Flanks profiles. E4N has plasma that extends up to high altitudes (800 km) and an unusual structure of essentially uniform density over 0–800 km altitude (as opposed to more traditional layer shapes). E45X also has plasma extending to high altitudes (400–600 km) and could be consistent either with a very broad layer of plasma or essentially uniform density over hundreds of km. Densities are slightly larger in E45X than E4N between 300 and 400 km (Figure S4 in Supporting Information S1), but uncertainties make it hard to say conclusively whether there is a difference. Overall, the ionosphere appears relatively stable and repeatable in the Night/Flanks sector.

This picture is consistent with model predictions by Bagenal and Dols (2020), with both Juno observations sitting on the flanks of Europa's magnetosphere, and with the egress point marginally closer to the magnetospheric wake, which could explain the higher ionospheric altitudes, but measurements from radio occultations estimate larger electron densities. Work by Harris et al. (2022) successfully reconciled the Galileo radio occultation observations as reported in Kliore et al. (1997) and McGrath et al. (2009) with models of the neutral atmosphere based on remote observations, by exploring different conditions for both scale height and atmospheric surface density. They found that both the electron density and the thickness of Europa's ionosphere increase with those parameters, and that this effect dominates over other sources of variability. In particular, a number of their models with higher O_2 surface densities and larger scale heights ($>100 \text{ km}$) are consistent with both the electron densities observed by Galileo and Juno (Figure S4 in Supporting Information S1), and the inferred neutral surface density from Kliore et al. (1997).

The largest Galileo densities were detected on E4X ($10,000 \text{ cm}^{-3}$, Day/Flanks), E6aN ($10,000 \text{ cm}^{-3}$, Day/Nose) and E6bN ($8,000 \text{ cm}^{-3}$, Day/Wake). The large signature retrieved during E6aN could be caused by the presence of a plume (McGrath & Sparks, 2017). That's all three of the Galileo dayside profiles, while the three Galileo nightside profiles all have smaller densities. Yet Juno's E45 N (Day/Flanks) has densities that are clearly smaller than $8,000 \text{ cm}^{-3}$. The same can be said for E45X (Night/Flanks), which is only slightly across the terminator. The Galileo profiles at $\text{SZA} = 85^\circ$ and 95° had a clear trend of large densities on the dayside, but the Juno profiles at $\text{SZA} = 89.3^\circ$ and 90.6° do not have as large densities as the Galileo profiles regardless of ram angle considerations. Nevertheless, it is challenging to arrive at definitive conclusions regarding ionospheric variabilities considering the significant uncertainties and the limited number of observations. Finally, E45X occurred within 5° latitude and 25° longitude of E4N, 25 years later. Although they were characterized by different SZA/ram conditions (Night/Flanks vs. Day/Flanks), both show plasma that extends up to high altitudes and similar electron densities around $\sim 5,000 \text{ cm}^{-3}$. However, we doubt this constitutes strong evidence of dependence from geographic location, except in the location of plumes where elevated densities may be present (McGrath & Sparks, 2017).

Kliore et al. (1997) reported an electron density scale height of $240 \pm 40 \text{ km}$ below 300 km, which has implications for temperatures in the neutral atmosphere. As for the Juno observations, the average electron density has an overall scale height of $405 \pm 205 \text{ km}$, consistent with Galileo's. However, uncertainties make this comparison of limited value. The E45X profile has a clear local maximum at an altitude above the surface, which implies that the neutral atmospheric density is large enough to put optical depth of one well above Europa's surface. Optical depth could apply to ionizing photons in the traditional sense or, if particle impact ionization dominates, to where magnetospheric particles are collisionally decelerated and stopped.

Data Availability Statement

The Juno radio science data used in this research are publicly available through NASA's Planetary Data System (Buccino, 2016). The occultation results presented here are provided in a corresponding data set with this publication on Zenodo (Parisi et al., 2023).

Acknowledgments

The work of DRB, MP, RSP, and SL was carried out at the Jet Propulsion Laboratory, California Institute of Technology, under a contract with the National Aeronautics and Space Administration (80NM0018D0004). Government sponsorship acknowledged. AC, EG, LGC, PT, and MZ are grateful to the Italian Space Agency for financial support through Agreement No. 2018-25-HH.0 in the context of ESA's JUICE mission, and Agreement No. 2017-40-H.1-2020, and its extension 2017-40-H.02020-13-HH.0, for ESA's BepiColombo and NASA's Juno radio science experiments. EG is grateful to "Fondazione Cassa dei Risparmi di Forlì" for financial support of his PhD fellowship. PW and DC acknowledge support from NASA award 80NSSC23K0020. PS was supported by NASA Contract NNM06AA75C from the Marshall Space Flight Center under subcontract 699054X from Southwest Research Institute. © 2023. All rights reserved.

References

- Asmar, S. W., Bolton, S. J., Buccino, D. R., Cornish, T. P., Folkner, W. M., Formaro, R., et al. (2017). The Juno gravity science instrument. *Space Science Reviews*, 213(1), 205–218. <https://doi.org/10.1007/s11214-017-0428-7>
- Bagenal, F., & Dols, V. (2020). The space environment of Io and Europa. *Journal of Geophysical Research: Space Physics*, 125(5), e2019JA027485. <https://doi.org/10.1029/2019ja027485>
- Bourgoin, A., Gramigna, E., Zannoni, M., Casajus, L. G., & Tortora, P. (2022). Determination of uncertainty profiles in neutral atmospheric properties measured by radio occultation experiments. *Advances in Space Research*, 70(8), 2555–2570. <https://doi.org/10.1016/j.asr.2022.07.015>
- Bourgoin, A., Zannoni, M., & Tortora, P. (2019). Analytical ray-tracing in planetary atmospheres. *Astronomy and Astrophysics*, 624, A41. <https://doi.org/10.1051/0004-6361/201834962>
- Buccino, D. R. (2016). Juno Jupiter gravity science raw data set V1.0 [Dataset]. JUNO-J-RSS-1 JUGR-V1.0, NASA planetary data system (PDS). https://atmos.nmsu.edu/PDS/data/jnogr_v1_001/
- Buccino, D. R., Parisi, M., Gramigna, E., Gomez-Casajus, L., Tortora, P., Zannoni, M., et al. (2022). Ganymede's ionosphere observed by a dual-frequency radio occultation with Juno. *Geophysical Research Letters*, 49(23), e2022GL098420. <https://doi.org/10.1029/2022gl098420>
- Caruso, A., Bourgoin, A., Togni, A., Zannoni, M., & Tortora, P. (2023). Radio occultation data analysis with analytical ray-tracing. *Radio Science*, 58(9), e2023RS007740. <https://doi.org/10.1029/2023rs007740>
- Dalba, P. A., & Withers, P. (2019). Cassini radio occultation observations of Titan's ionosphere: The complete set of electron density profiles. *Journal of Geophysical Research: Space Physics*, 124(1), 643–660. <https://doi.org/10.1029/2018ja025693>
- Fjeldbo, G., & Eshelman, V. R. (1968). The atmosphere of Mars analyzed by integral inversion of the Mariner IV occultation data. *Planetary and Space Science*, 16(8), 1035–1059. [https://doi.org/10.1016/0032-0633\(68\)90020-2](https://doi.org/10.1016/0032-0633(68)90020-2)
- Gomez Casajus, L., Zannoni, M., Modenini, D., Tortora, P., Nimmo, F., Van Hoolst, T., et al. (2021). Updated Europa gravity field and interior structure from a reanalysis of Galileo tracking data. *Icarus*, 358, 114187. <https://doi.org/10.1016/j.icarus.2020.114187>
- Gramigna, E., Parisi, M., Buccino, D., Casajus, L. G., Zannoni, M., Bourgoin, A., et al. (2023). Analysis of NASA's DSN Venus Express radio occultation data for year 2014. *Advances in Space Research*, 71(1), 1198–1215. <https://doi.org/10.1016/j.asr.2022.10.070>
- Grima, C., Blankenshio, D. D., & Schroeder, D. M. (2015). Radar signal propagation through the ionosphere of Europa. *Planetary and Space Science*, 117, 421–428. <https://doi.org/10.1016/j.pss.2015.08.017>
- Hall, D. T., Strobel, D. F., Feldman, P. D., McGrath, M. A., & Weaver, H. A. (1995). Detection of an oxygen atmosphere on Jupiter's moon Europa. *Nature*, 373(6516), 677–679. <https://doi.org/10.1038/373677a0>
- Hansen, C. J., Bolton, S., Sulaiman, A. H., Duling, S., Bagenal, F., Brennan, M., et al. (2022). Juno's close encounter with Ganymede—An overview. *Geophysical Research Letters*, 49(23), e2022GL099285. <https://doi.org/10.1029/2022gl099285>
- Harris, C. D. K., Jia, X., & Slavin, J. A. (2022). Multi-fluid MHD simulations of Europa's plasma interaction: Effects of variation in Europa's atmosphere. *Journal of Geophysical Research: Space Physics*, 127(9), e2022JA030569. <https://doi.org/10.1029/2022ja030569>
- Juno Navigation Team. (2022). The JUNO SPICE data archive [Dataset]. PDS Navigation and Ancillary Information Facility (NAIF) Node. https://naif.jpl.nasa.gov/pub/naif/pds/data/jno-j_e_ss-spice-6-v1.0/
- Kliore, A. J. (1998). Satellite atmospheres and magnetospheres. *Highlights of Astronomy*, 11(2), 1065–1069. https://doi.org/10.1007/978-94-011-4778-1_138
- Kliore, A. J., Cain, D. L., Levy, G. S., Eshleman, V. R., Fjeldbo, G., & Drake, F. D. (1965). Occultation experiment: Results of the first direct measurement of Mars's atmosphere and ionosphere. *Science*, 149(3689), 1243–1248. <https://doi.org/10.1126/science.149.3689.1243>
- Kliore, A. J., Cain, Fjeldbo, D. L. G., Seidel, B. L., & Rasool, S. I. (1974). Preliminary results on the atmospheres of Io and Jupiter from the Pioneer 10 S-band occultation experiment. *Science*, 183(4122), 323–324. <https://doi.org/10.1126/science.183.4122.323>
- Kliore, A. J., Hinson, D. P., Flasar, F. M., Nagy, A. F., & Cravens, T. E. (1997). The ionosphere of Europa from Galileo radio occultations. *Science*, 277(5324), 355–358. <https://doi.org/10.1126/science.277.5324.355>
- Mazarico, E., Buccino, D., Castillo-Rodriguez, J., Dombard, A. J., Genova, A., Hussmann, H., et al. (2023). The Europa clipper gravity and radio science investigation. *Space Science Reviews*, 219(4), 30. <https://doi.org/10.1007/s11214-023-00972-0>
- McGrath, M. A., Hansen, C. J., & Hendrix, A. R. (2009). Observations of Europa's tenuous atmosphere. In R. T. Pappalardo, W. B. McKinnon, & K. K. Khurana (Eds.), *Europa* (chap. 20). University of Arizona Press.
- McGrath, M. A., & Sparks, W. B. (2017). Galileo ionosphere profile coincident with repeat plume detection location at Europa. *Research Notes of the AAS*, 1, 14. <https://doi.org/10.3847/2515-5172/aa988e>
- Moirano, A., Gomez Casajus, L., Zannoni, M., Durante, D., & Tortora, P. (2021). Morphology of the Io plasma torus from Juno radio occultations. *Journal of Geophysical Research: Space Physics*, 126(10), e2021JA029190. <https://doi.org/10.1029/2021ja029190>
- Paik, M., & Asmar, S. W. (2010). Detecting high dynamics signals from open-loop radio science investigations. *Proceedings of the IEEE*, 99(5), 881–888.
- Parisi, M., Caruso, A., Buccino, D. R., Gramigna, E., Withers, P., Gomez-Casajus, L., et al. (2023). Corresponding dataset for “measurements of Europa's ionosphere from Juno's close flyby” (version V1) [Dataset]. Zenodo. <https://doi.org/10.5281/zenodo.8381465>
- Phinney, R. A., & Anderson, D. L. (1968). On the radio occultation method for studying planetary atmospheres. *Journal of Geophysical Research*, 73(5), 1819–1827. <https://doi.org/10.1029/ja073i005p01819>
- Phipps, P. H., Withers, P., Buccino, D. R., Yang, Y., & Parisi, M. (2021). Two years of observations of the Io plasma torus by Juno radio occultations: Results from Perijoves 1 to 15. *Journal of Geophysical Research: Space Physics*, 126(3), e2020JA028710. <https://doi.org/10.1029/2020ja028710>
- Schinder, P. J., Flasar, F. M., Marouf, E. A., French, R. G., Anabtawi, A., Barbinis, E., & Kliore, A. J. (2015). A numerical technique for two-way radio occultations by oblate axisymmetric atmospheres with zonal winds. *Radio Science*, 50(7), 712–727. <https://doi.org/10.1002/2015rs005690>
- Togni, A., Zannoni, M., Casajus, L. G., & Tortora, P. (2021). An FFT-based method for Doppler observables estimation in Deep Space tracking. In *2021 IEEE 8th International Workshop on Metrology for AeroSpace (MetroAeroSpace)* (pp. 294–299). IEEE.
- Withers, P., & Moore, L. (2020). How to process radio occultation data: 2. From time series of two-way, single-frequency frequency residuals to vertical profiles of ionospheric properties. *Radio Science*, 55(8), 1–25. <https://doi.org/10.1029/2019rs007046>